Photoenhanced Water Electrolysis in Separate O_2 and H_2 Cells Using Pseudocapacitive Electrodes

Supansa Musikajaroen, Siwat Polin, Suchinda Sattayaporn, Warakorn Jindata, Wittawat Saenrang, Pinit Kidkhunthod, Hideki Nakajima, Teera Butburee, Narong Chanlek, and Worawat Meevasana*

Cite This: *ACS Omega* 2021, 6, 19647−19655

Read Online

ACCESS | Metrics & More | Article Recommendations | Supporting Information

ABSTRACT: Water electrolysis has received much attention in recent years as a means of sustainable H_2 production. However, many challenges remain in obtaining high-purity H_2 and making large-scale production cost-effective. This study provides a strategy for integrating a two-cell water electrolysis system with solar energy storage. In our proposed system, $CuO\text{-}Cu(OH)_2/Cu_2O$ was used as a redox mediator between oxygen and hydrogen evolution components. The system not only overcame the gas-mixing issue but also showed high gas generation performance. The redox reaction (charge/discharge) of $CuO\text{-}Cu(OH)_2/Cu_2O$ led to a significant increase (51%) in the initial rate of H_2 production from 111.7 μmol h^{-1} cm^{-2} in the dark to 168.9 μmol h^{-1} cm^{-2} under solar irradiation. The effects of light on the redox reaction of $CuO\text{-}Cu(OH)_2/Cu_2O$ during water electrolysis were investigated by in situ X-ray absorption and photoemission spectroscopy. These results suggest that surface oxygen vacancies are created under irradiation and play an important role in increased capacitance and gas generation. These findings provide a new path to direct storage of abundant solar energy and low-cost sustainable hydrogen production.
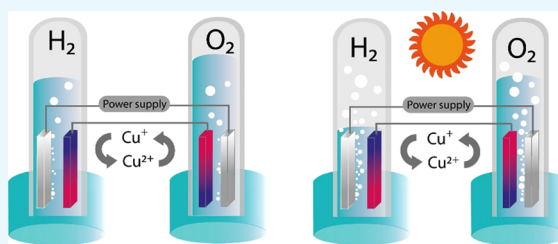
INTRODUCTION

Water electrolysis provides a promising path for sustainable hydrogen production because it stands out as a mature, scalable technology for which the only required inputs are water and energy (in the form of electricity).[1] However, both improving the yield of high-purity H_2 and reducing the production cost remain challenges to the application of water electrolysis for large-scale hydrogen production.[2−5] Therefore, water electrolysis in separate cells combined with renewable solar energy provides an alternative path for efficient device design and reduction of the cost of H_2 production.

In conventional water electrolysis, hydrogen and oxygen gases are simultaneously produced in the same cell. Mixing of these gases can occur during electrolysis, resulting in the degradation of electrolyzers as well as raising safety concerns.[6,7] Therefore, several methods to prevent the mixing of gaseous H_2 and O_2 products are proposed.[4−6,8−13] Cronin's group suggested a new method to separate gases produced in the conventional proton exchange membrane (PEM) water electrolysis process using a soluble molecular redox mediator (silicotungstic acid) that mediates the electron-coupled proton exchange between the oxygen and hydrogen evolution reactions (OER and HER, respectively).[9,10] Although PEM water electrolysis systems offer several advantages,[9,10,14,15] their application remains hampered by the low efficiency and high cost of the Pt catalysts and membranes.[11] To overcome these problems, the separation of H_2 and O_2 production using $Ni(OH)_2/NiOOH$ redox mediator electrodes in alkaline

aqueous solution was proposed.[4,5,8,13] In this setup, the two separate cells use the redox reaction of $Ni(OH)_2/NiOOH$ to mediate the ion exchange where there is a copper wire linking the two mediator electrodes instead of a membrane.[4,5] Compared with PEM water electrolysis, alkaline water electrolysis exhibits inherent low-cost characteristics because it can use a nonprecious catalyst and a porous separator. The overall efficiency of water splitting in alkaline media would be better than that in acidic media.[11] Moreover, Rothschild's team provided the concept of using solar power to drive the separation of H_2 and O_2 production in this two-cell setup.[4] In this work, we would firstly look into another oxide material (i.e., $CuO\text{-}Cu(OH)_2/Cu_2O$) that can be used as a redox mediator, and with Rothschild's concept of solar power, we would also like to investigate if the gas production can be further enhanced via the solar irradiation of the mediator electrodes.

The CuO, $Cu(OH)_2$, and Cu_2O electrodes have been widely used in rechargeable batteries and pseudocapacitors using alkaline electrolytes due to their high redox reaction and specific capacitance.[16−19] Therefore, the redox-reversible CuO-
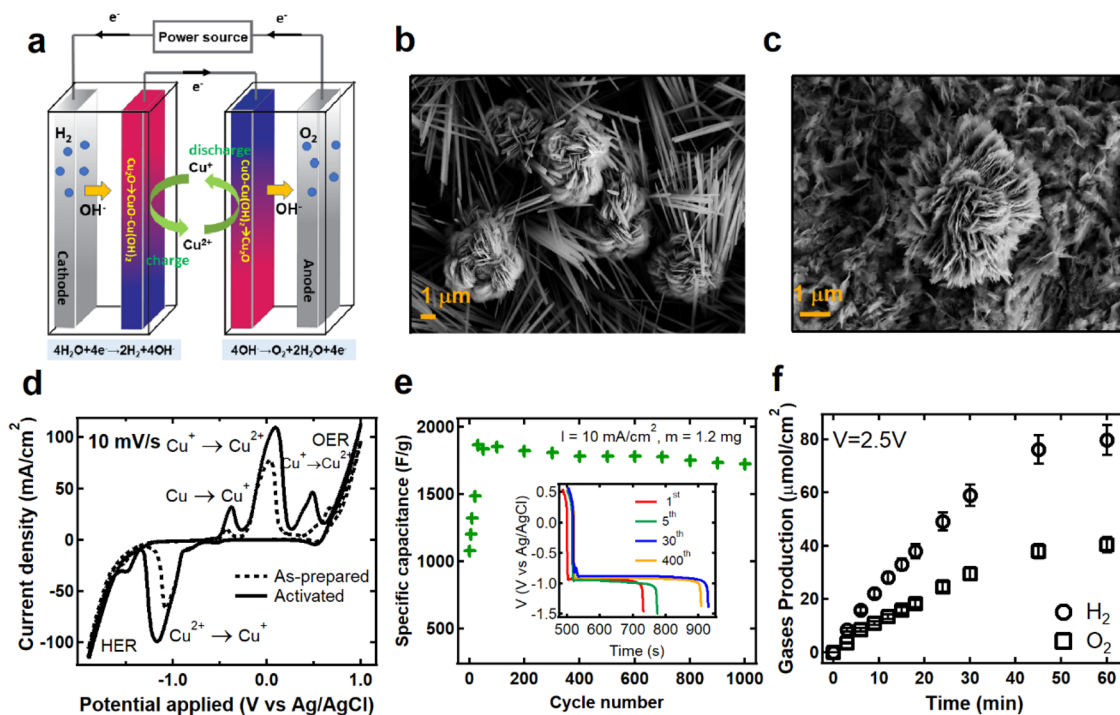
Figure 1. Redox mediator electrodes and experimental setup. (a) Schematic diagram of the electrolysis system. (b) SEM image of the CuO-Cu(OH)$_2$ as-prepared electrode directly grown onto a copper foil via surface oxidation in alkaline solution. At the reaction time of 30 min, the CuO micro-flowers are standing on Cu(OH)$_2$ nanowire arrays. (c) SEM image of the CuO-Cu(OH)$_2$ electrode after the activation process that included 300 activation cycles with charge and discharge steps at a constant current of 30 mA (3 mA/cm^2). After activation, the Cu(OH)$_2$ nanowire transformed to CuO flower petals with a nanoscale thickness. (d) CV curves of CuO-Cu(OH)$_2$ electrode before and after the activation process at 10 mV/s with potential range from −2 to 1 V vs Ag/AgCl. (e) The cycling stability and galvanostatic discharge curves (inset) of the CuO-Cu(OH)$_2$/Cu-foil electrode by charge/discharge measurement at 10 mA/cm^2 and −1.4−0.6 V vs Ag/AgCl in 1 M NaOH. (f) H$_2$ and O$_2$ production that evolved during operation at a potential bias of 2.5 V in the two-cell water electrolysis that was set up according to the schematic diagram in (a).

Cu(OH)$_2$/Cu$_2$O electrodes are suitable to be used as an ion exchange mediator in our two-cell water electrolysis system. The electrons transfer from one mediator electrode to another by the charge and discharge processes of mediator electrodes. Therefore, the capacitance of mediator electrodes has an important influence on the electrolysis rate in the two-cell water splitting system. Many studies report that charging and discharging of supercapacitive hydroxides and oxides under illumination can provide a higher areal current and capacitance due to photogenerated electron−hole pairs in the electrode materials.[20−24] Compared with NiOOH/Ni(OH)$_2$, using CuO-Cu(OH)$_2$/Cu$_2$O as mediator electrodes could easily enhance the performance of a two-cell water electrolysis system by illumination due to its narrow band gap. It therefore strongly absorbs solar irradiation,[25−28] which enables the generation of electron−hole pairs for enhanced redox and charge transfer in the water splitting system.

Herein, we present a concept providing a significant enhancement in the production of pure gases in a two-cell water electrolysis system by using charge−discharge Cu$_2$O/CuO-Cu(OH)$_2$ redox mediator electrodes under solar irradiation. In this work, the hydrogen and oxygen cells are separated by using CuO-Cu(OH)$_2$/Cu$_2$O mediator electrodes which substitute membrane separator for ion exchange between the anode and cathode. The CuO-Cu(OH)$_2$ (mixture of CuO and Cu(OH)$_2$) converts to Cu$_2$O during O$_2$ production at the anode ($4OH^- \rightarrow O_2 + 2H_2O + 4e^-$), while Cu$_2$O simultaneously converts to CuO-Cu(OH)$_2$ during H$_2$ production at the cathode ($4H_2O + 4e^- \rightarrow 2H_2 + 4OH^-$).

This system, the CuO-Cu(OH)$_2$ with Cu$_2$O, has both photosensitive and pseudocapacitive properties. The capacitance of mediator electrodes is improved greatly under light illumination by the creation of surface oxygen vacancies in the Cu$_2$O electrode. Therefore, the solar power can be captured and directly stored. This concept provides a new way of sustainable hydrogen production while reducing costs for large-scale utilization.

■ RESULTS

A CuO-Cu(OH)$_2$/Cu$_2$O redox couple was used as a mediator electrode in a two-cell water electrolysis system, as shown in the schematic in Figure 1a. The Cu$_2$O is used in the hydrogen production cell, and CuO-Cu(OH)$_2$ is used in the oxygen production cell. Electrons are transferred from Cu$_2$O to CuO-Cu(OH)$_2$, and ions (OH$^-$) are exchanged between the primary electrodes (cathode and anode) by the charging and discharging of the Cu$_2$O/CuO-Cu(OH)$_2$ mediator electrodes. This process is accompanied by a visible color change from red to dark blue (see Figure S1a in the Supplementary Information). The charge and discharge cycle of the mediator pair depends on the reversible transformation of CuO-Cu(OH)$_2$/Cu$_2$O, which typically falls within the potential range of −1.5 to 0.7 V.[17,19,29−31] The electrochemical reactions are as follows:

$$Cu_2O + 2OH^- + H_2O \leftrightarrow 2Cu(OH)_2 + 2e^- \tag{1}$$

$$Cu_2O + 2OH^- \leftrightarrow 2CuO + H_2O + 2e^- \tag{2}$$
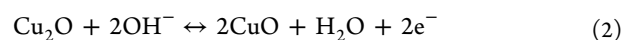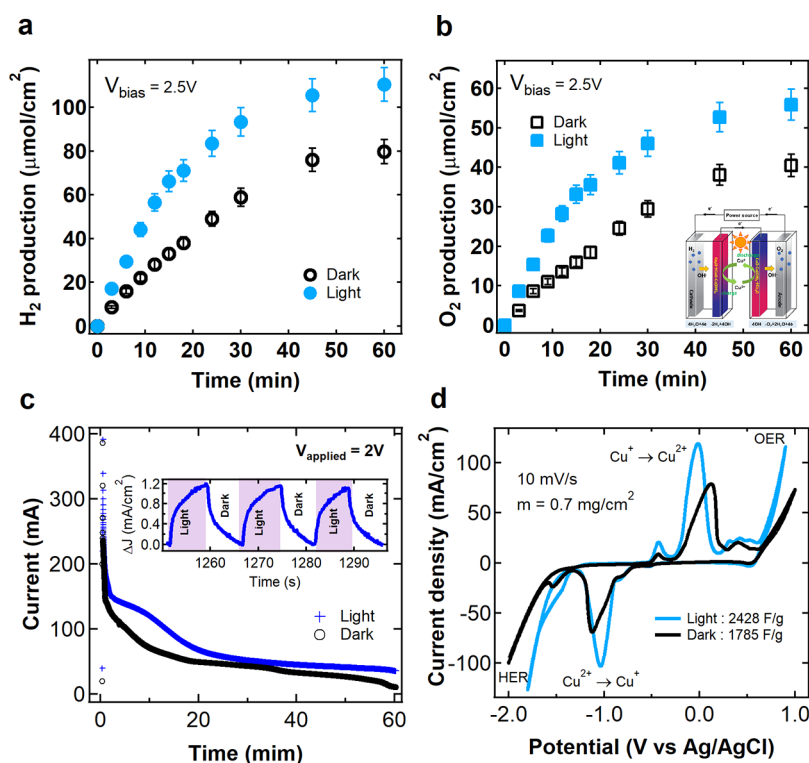
Figure 2. Effect of sunlight on CuO-Cu(OH)$_2$/Cu$_2$O redox mediator electrode. (a, b) H$_2$ and O$_2$ production in the two-cell water electrolysis system operated at a potential application of 2.5 V under dark and sunlight illumination. The sunlight was shone on the redox electrode (as shown in the inset (b)). (c) Current density of the two-cell water electrolysis system under sunlight conditions. The inset shows the additional current density depending on light on or off. (d) CV curve of the CuO-Cu(OH)$_2$ electrode at 10 mV/s in a three-electrode system under dark and sunlight illuminations.

To ensure the stability of the process during electrolysis, our CuO-Cu(OH)$_2$ electrodes were activated using the continuous charge/discharge process prior to fabricating the electrolytic cell. After activation, Cu(OH)$_2$ nanowires transform to CuO nanosheets with a thickness of approximately 50−100 nm as shown in Figure 1b,c, respectively (see details in Figures S2−S4). The changing of morphology provides a large electrode−electrolyte interface for an efficient redox reaction (see cyclic voltammetry (CV) curves in Figure 1d). The charge transfer and electrolyte diffusion resistance are smaller (Figure S5), leading to its specific capacitance in a potential range of −1.3−0.6 V vs Ag/AgCl that becomes larger than that of the as-prepared electrode (Figure 1e).

To start the electrolysis process, a constant voltage (2.5 and 3.0 V) was applied across the device for 1 h. Bubbles indicated the evolution of gaseous H$_2$ and O$_2$ at the cathode and anode, respectively, while there were no bubbles that formed at the mediator electrodes (Supplementary Note 6). The volume of gas evolved as a function of time at V = 2.5 V is shown in Figure 1f. The initial rates during the first 30 min are 111.7 and 57.2 μmol h^{-1} cm^{-2} (average rates of HER and OER are 74.9 and 38.7 μmol h^{-1} cm^{-2}); the H$_2$-to-O$_2$ ratio is approximately 2:1 in the consecutive cycles, similar to the previous studies.[4,6] The production rate of H$_2$ and O$_2$ depends on the electrode's SOC (state of charge) (see Supplementary Note 7). Upon increasing the run time, the mediator electrode will be closer to the fully discharged state where the gas production will be stopped. Then, after approximately 1.2 h, the mediator electrode pair was nearly fully charged/discharged. Subsequent electrolysis could then be resumed by switching the applied voltage between the anode and cathode. Correlation of the

quantity of gas produced with the charge passed during electrolysis showed good average electrolysis efficiency ($\eta_V = V_{rev}/V_{appl}$) of 47% (see Supplementary Note 1) and Faradaic efficiency of approximately 95 ± 2% (H$_2$ production) and 95% ± 4% (O$_2$ production) (Figure S8a), comparable to the Ni(OH)$_2$/NiOOH mediator pair studied in refs 2, 4. Deviation of the measured Faradaic efficiency from a theoretically achievable 100% yield is most likely due to a combination of gas leakage and dissolution of H$_2$ in the aqueous solution.

The cyclic stability of CuO-Cu(OH)$_2$/Cu$_2$O mediator electrodes (measurement area 1 cm^2) was investigated by continuous charging and discharging for 1000 cycles at a current density of 10 mA/cm^2 (8.3 A/g) in 1 M NaOH solution within the potential range of −1.4−0.6 V vs Ag/AgCl. The specific capacitance curve shows a good retention rate as shown in Figure 1e where the specific capacitance remains to be at 1725 F/g after 1000 cycles or around 92% compared to that of the initially activated electrode (highest specific capacitance is 1867 F/g). During the charge−discharge process, the morphology of the mediator electrodes before and after looks similar to each other (Figure S2g,h), in agreement with the good retention, while some small degradation may come from the Cu(I)/Cu(0) reaction. Regarding the stability of the electrolysis system, the cycle duration as a function of cycle number is shown in Figure S9. The cycle duration decreases by only 7.5% after 55 electrolysis cycles, which is a good sign for the two-cell electrolysis system compared to the previous study.[4]

Interestingly, solar irradiation of the mediator electrodes during the charge and discharge processes led to an increase in the evolution rate of both H$_2$ and O$_2$ gases. As shown in Figure
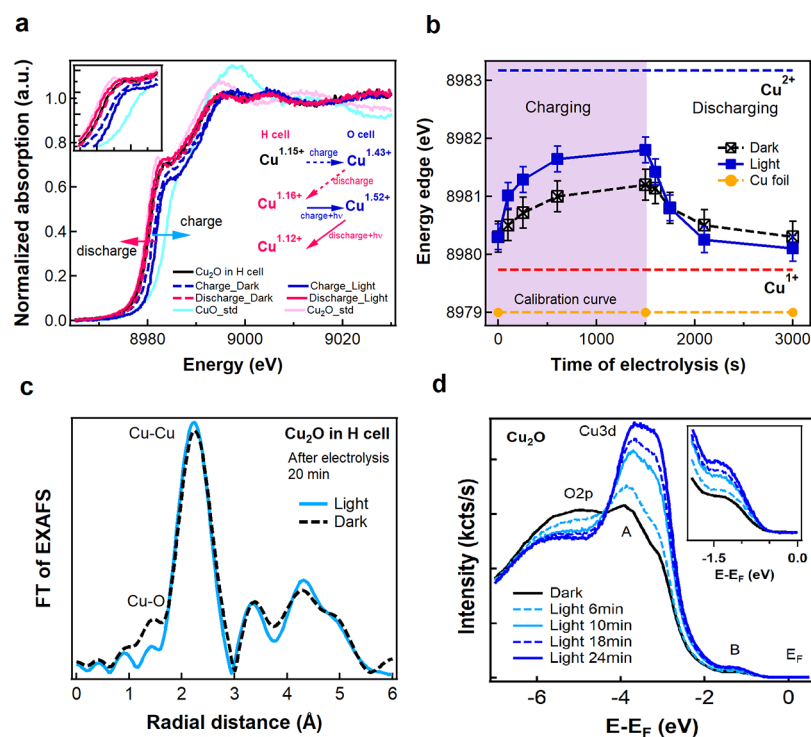
Figure 3. Electronic structure of CuO-Cu(OH)$_2$/Cu$_2$O redox mediator electrode. (a) In situ Cu K-edge fluorescence XANES spectra of the mediator electrode during charging and discharging under dark and light illuminations in two-cell water electrolysis at 3 V. The changing of oxidation state for each condition is shown in the inset. (b, c) Changing absorption edge positions and FT EXAFS structures of redox mediator electrodes during charging and discharging under dark and light illumination. (d) Evolution of the valence band (VB) spectra of the Cu$_2$O redox mediator electrode from the pristine fractured surface to the light irradiated surface. Inset shows the evolution of the in-gap state with increasing exposure time.

2a,b, H$_2$ and O$_2$ were evolved at 110.4 and 55.8 μmol h^{-1} cm^{-2}, representing an increase of approximately 38%, while initial evolution rates at 30 min increase up to 51%. This reflects a corresponding increase in the charge transfer ($Q = \int Idt$) between the anode and cathode (see Figure 2c), rising from 46 mAh in the absence of irradiation to 64 mAh under solar irradiation. The effect of solar irradiation was also studied by testing the two-cell water electrolysis under light on–off conditions. As shown in Figure 2c and inset, additional current density was observed when the CuO-Cu(OH)$_2$ and Cu$_2$O redox electrodes were operated under solar irradiation. This confirms that the presence of sunlight improves the yield of H$_2$ production.

To further elucidate the effect of solar irradiation on our system, the electrochemical properties of the CuO-Cu(OH)$_2$/Cu$_2$O mediator pairs were investigated. The resulting cyclic voltammetry (CV) measurement is shown in Figure 2d. This further supports evidence that the CuO-Cu(OH)$_2$/Cu$_2$O redox electrode provides a higher current density and specific capacitance under light irradiation. Photogenerated charge carriers drive the oxidation and reduction of Cu$_2$O/CuO-Cu(OH)$_2$ redox electrodes, leading to an enhancement of the specific capacitance by 36% compared with that in the absence of light.[20−22,24]

The changing oxidation states in the CuO-Cu(OH)$_2$/Cu$_2$O mediator electrode were tracked using in situ X-ray absorption spectroscopy (XAS) during charging and discharging in the presence and absence of solar irradiation. Figure 3a,b shows the resulting normalized Cu K-edge XANES spectra and the changes in the edge positions in the CuO-Cu(OH)$_2$/Cu$_2$O mediator electrode, which was tracked during the electrolysis.

The position of the absorption edge contains information on the electronic structure of Cu within the electrode. During the charging process of Cu$_2$O in the hydrogen cell, XANES spectra showed a clear shift to higher-energy states (see blue dash lines in Figure 3a). This indicates a change in the Cu oxidation state from +1.15 to +1.43 during electrolysis at 3 V for 30 min. A shift of the XANES spectra in the opposite direction (see red lines in Figure 3a) was observed during the discharging process of CuO-Cu(OH)$_2$ in the oxygen cell. The oxidation state of Cu was reduced back to +1.16, which is near the initial oxidation state (+1.15). These observations indicate the reversibility of redox in CuO-Cu(OH)$_2$/Cu$_2$O mediator electrodes. The changes in oxidation state during the charge and discharge processes are similar to those of other transition metal oxides in previous reports.[32,33] Interestingly, under light irradiation at 3 V on the mediator electrode during the charging process in the electrolysis system, the XANES Cu K-edge energy significantly shifts according to oxidation of +1.16 to +1.52 (see blue spectra in Figure 3a,b). During the discharge process of the mediator electrode, a lower energy edge upon light irradiation (see red spectra in Figure 3a,b) indicated an increased amount of Cu^{1+}, with the average oxidation number changing from +1.52 to +1.12. This change of oxidation state is consistent with our CV measurements.

The Fourier transform of Cu K-edge EXAFS spectra of Cu$_2$O during electrolysis under dark and light conditions provides coordination information from the radial distribution function (RDF), which is shown in Figure 3c (see more details in Supplementary Note 10). The first peak at about 1.45 Å corresponds to the nearest neighbor to Cu and therefore originates from Cu—O bonds. The peak at 2.24 Å matches

well with Cu—Cu bonds in the Cu foil substrate, which is consistent with previous reports.[34,35]

During the charging process (i.e., during electrolysis) under light irradiation, the radial distribution function obtained from EXAFS of the Cu_2O electrode showed a slight decrease in Cu—O bond length compared with the same measurement performed under dark conditions (see Supplementary Note 10). This effect can be seen in Figure 3c and corresponds to a significant change in the Cu—O coordination number resulting from fewer oxygen atoms as nearest neighbors. However, this effect was not observed in the case of CuO-Cu(OH)$_2$ electrode.

By using photoemission spectroscopy (PES), the electronic structure of the mediator electrode under illumination was also measured, which helps to elucidate the reaction mechanism at the electrodes during electrolysis. Figure 3d shows the valence band spectra of the Cu_2O mediator electrode with different carrier-dopants. It is clear that the valence band maximum is slightly shifted toward the Fermi level and the ratio of the Cu3d state (1.5−4 eV) to the O2p state (4−8 eV)[36] increases with increased carrier doping. This suggests a surface electron accumulation. It also indicates that electrons can be transferred from Cu_2O in the hydrogen cell to CuO-Cu(OH)$_2$ in the oxygen cell. This is consistent with the increase of current density in the CV curve and XAS results.

■ DISCUSSIONS

In a two-cell water electrolysis system, the CuO-Cu(OH)$_2$ and Cu_2O present both pseudocapacitive and photosensitive behaviors with high specific capacitance and excellent cycling stability. The integration of photosupercapacitive behavior with a mediator system in a single electrode offers important advantages. Specifically, the rate of evolution of H_2 and O_2 gases is significantly increased during sunlight irradiation onto the mediator electrodes. This is because the sunlight has an important influence on the pseudocapacitance behavior (Figure 2d). The solar power can be captured and directly stored chemically in redox mediator electrodes.

Under light irradiation, the charge in the electrolysis system was increased by 39% compared to that under dark conditions. In turn, the initial H_2 and O_2 evolution rates were significantly enhanced up to 51%. However, this effect depends strongly on which electrode is irradiated, as shown in the supplementary material (Figure S11). Irradiation of either the Cu_2O electrode alone or both electrodes at once produces a similar increase in gas evolution. On the other hand, when only the CuO-Cu(OH)$_2$ electrode in the oxygen cell is irradiated, there is a much weaker increase in the rate of gas evolution. This is because the conduction band minimum (CBM) of Cu_2O is higher in energy than the CBM of CuO.[35,37] Therefore, during the charge/discharge process, photogenerated electrons can easily transfer from Cu_2O to CuO but not the other way around.

The redox mechanism of the Cu_2O and CuO-Cu(OH)$_2$ mediator electrode pair during the charging/discharging process under light illumination in two-cell electrolysis involves a photoassisted charging mechanism of electrodes. During the charging process in the hydrogen cell, the valence electrons of Cu_2O are excited to the conduction band under light illumination, resulting in the generation of electron−hole pairs (eq 3). The holes accumulate at the Cu_xO/water interface and oxidize Cu_2O into CuO (eq 4).[20,38−43] Simultaneously, the photogenerated electrons pass through

the external circuit[18,22] to reduce the CuO-Cu(OH)$_2$ electrode in the oxygen cell. During the discharge process in the oxygen cell, CuO-Cu(OH)$_2$ can be reduced back to Cu_2O by following a reversible redox reaction process (eq 5).

The redox mechanism under light irradiation is as follows:[20,39,42]

$$Cu_2O \overset{h\nu}{\leftrightarrow} Cu_2O^+ + e^- \tag{3}$$

$$Cu_2O^+ + 2OH^- \leftrightarrow 2CuO + H_2O \tag{4}$$

$$Cu_2O + 2OH^- \overset{h\nu}{\leftrightarrow} 2CuO + H_2O + 2e^- \tag{5}$$
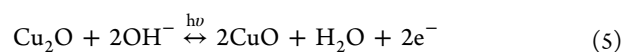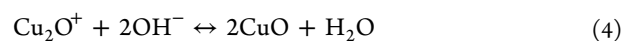
More importantly, during light illumination, the photo-generated holes with oxidation react with mediator electrodes. This promotes the utilization of the electrode materials and further enhances the specific capacitance.

In situ Cu K-edge XANES was used to study the local electronic structure of redox mediator electrodes during electrolysis at a constant system voltage of 3 V. Upon light irradiation of the Cu_2O mediator electrode in the hydrogen cell, a larger shift of the Cu K-edge energy (Figure 3b) during charging indicated a greater positive shift in the oxidation state of Cu compared with the same experiment performed in the absence of light. This suggests that the photogenerated holes[44,45] in the Cu_2O electrode assisted the oxidation of Cu_2O to CuO-Cu(OH)$_2$. On the other hand, the reduction of the Cu oxidation state in CuO-Cu(OH)$_2$ during the discharging process under irradiation suggests the migration of electrons from the Cu_2O electrode to the CuO-Cu(OH)$_2$ electrode. These electrons consequently reduced CuO-Cu-(OH)$_2$ to Cu_2O. The reduction was more pronounced under light irradiation due to the difference in charge storage between dark and light conditions. These results confirm the photoassist charging of the mediator electrodes during water electrolysis, which is in good agreement with electrochemical results.

The Fourier transforms of Cu K-edge EXAFS spectra (shown in Figure 3c) of Cu_2O during electrolysis under dark and light conditions were also studied to support the observations made from XANES. Interestingly, the only significant change in these arose from shifts in the Cu—O bond peak. A lower coordination number of Cu—O bonds under irradiation is indicated, suggesting that oxygen vacancies[46,47] are created in the Cu_2O electrode during electrolysis under light irradiation.

Electronic change local to the surface of the redox mediator electrodes was also tracked by taking both the valence band and XPS photoemission spectra of Cu_2O and CuO-Cu(OH)$_2$ during irradiation (Figure 3d and Figure S12 and S13, respectively). As exposure time increased, the O2p state decreases and its leading edge shifts slightly toward the Fermi level. It is accompanied by an increase in the intensity of the sub-gap state peak around 1.3 eV (inset in Figure 3d). Looking at previous studies, we consider that this sub-gap defect state is most likely associated with oxygen vacancies at the sur-face.[48−52] The surface oxygen vacancies on Cu_2O electrodes play an important role in the separation of photogenerated electron−hole pairs and in the improvement of redox behavior involving photocapacitive performance.[51−58] When Cu_2O is irradiated by light greater than its optical bandgap (valence band maximum (VBM) shift to EF), electron−hole pairs are generated (eq 3). Then, the photogenerated electrons are

trapped by surface oxygen vacancies (peak at 1.3 eV).[54,55,59] These charges captured momentarily by surface oxygen vacancies are then readily transmitted to the Cu substrate[55,60] (see schematic in Figure S14). Meanwhile, the photogenerated holes act to oxidize Cu_2O to CuO and H_2O as in eq 4. Our spectroscopic observations are consistent with the capacitive improvement of the mediator electrodes under solar irradiation as demonstrated in the CV curve. Importantly, oxygen vacancies enhance the electrical conductivity of transition metal oxides[50,58] as a mediator electrode. The electron–hole pairs can be efficiently separated (inset in Figure 2c), resulting in higher gas evolution rates compared to those in the absence of light.

CONCLUSIONS

In conclusion, a two-cell electrolytic water splitting system has been developed with electrodes acting both as a redox mediator and as a photosupercapacitor for improved H_2 and O_2 gas production. The solar-driven pseudocapacitive behavior on the CuO-$Cu(OH)_2$/Cu_2O mediator electrode pair exhibits an increase in the specific capacitance compared with that in the absence of light (36%). This implies direct storage of solar energy that provided an increase in the initial H_2 and O_2 production rates of 51%. Our observations indicate that as a Cu_2O electrode is irradiated with solar light in a hydrogen cell, surface-localized oxygen vacancies are created. These play an important role in the separation of photogenerated electron–hole pairs, providing an improvement of redox behavior and capacitive activity in our two-cell water electrolysis system.

Regarding its application, this work provides a new strategy of combining a two-cell water electrolysis system with a photosupercapacitor in one device that is a route to low-cost and sustainable hydrogen production. Firstly, the two-cell system requires no expensive proton exchange membranes (PEM) commonly used in water electrolysis systems. Furthermore, in our system, the free solar irradiation could boost the performance of H_2 production by 51% and effectively increase the energy storage capacity of the mediator electrode. The effective increase in this solar-enhanced capacity is important for the cost optimization since the effective cost of energy storage is usually many folds of the solar cell panels proposed as the clean electricity generator for the H_2 production system.

EXPERIMENTAL DETAILS

Synthesis and Characterization of the CuO-$Cu(OH)_2$ Electrode. The $Cu(OH)_2$ nanowire/microflower-like CuO films on Cu foil were synthesized by chemical oxidation. A Cu foil (9 μm, 99%, MTI USA) was cut into 2.5 × 5 cm^2 sheets and cleaned by ultrasonication (water bath, 240 W) in acetone, ethanol, and distilled water at room temperature for 10 min sequentially. Impurities and oxide layers were removed from the surface by immersing in 1 M HCl solution for 30 min.[19] The cleaned Cu foil was then immersed in an aqueous solution consisting of 24 mL of 10 M NaOH, 12 mL of 1 M $(NH4)_2S_2O_8$, and 54 mL of distilled water[19] at room temperature (25 °C). After 15–30 min, a dark-blue film covered the Cu foil surface, indicating the formation of $Cu(OH)_2$. The $Cu(OH)_2$-coated Cu foil was then taken from the solution, rinsed with water and then ethanol, and dried in air.

The morphology and chemical composition of the $Cu(OH)_2$ nanowire/microflower-like CuO were examined by scanning electron microscopy (SEM, ZEISS Auriga, operated at 5 keV) and energy-dispersive X-ray spectroscopy (EDS) (see Figures S2 and S3). The crystal structures of the samples were analyzed using an X-ray diffractometer (XRD, Bruker D2 Advance diffractometer) with Cu Kα radiation (λ = 0.1506 nm). The XRD patterns as shown in Figure S4 are measured with a scan rate of 10° min^{-1} at a step width of 0.02°.

Electrochemical Characterization and Electrode Activation. The electrochemical measurement and electrode activation were carried out on a potentiostat/galvanostat. The $Cu(OH)_2$ nanowire/microflower-like CuO redox electrode was used as the working electrode (WE) in an electrochemical cell operated in a conventional three-electrode system with a Pt counter electrode (CE) and an Ag/AgCl reference electrode (RE) in an aqueous electrolyte solution of 1 M NaOH in deionized water. During the activation process, the working electrode was charged and discharged until its discharge capacity stabilized. At the end of the activation process, one of the redox electrodes (size 2.5 × 4 cm^2) was charged and converted to CuO-$Cu(OH)_2$ by constant current charging (4 mA/cm^2, 1.5 h), whereas the other one (size 2.5 × 4 cm^2) was discharged and converted to Cu_2O by constant current discharging (−4 mA/cm^2, 1.5 h). In addition, the electrochemical measurement of half-cell electrodes (1 × 1 cm^2) was performed under dark and light illumination at 80 mW/cm^2 (approx. 0.8 Sun with 1.5 air mass) by using a PET solar simulator (model SS100AAA).

Two-Cell Water Electrolysis System. A two-cell water electrolysis system (shown in Figure 1a) was constructed with Ni foam primary electrodes (2.5 × 4 cm^2) and CuO-$Cu(OH)_2$/Cu_2O (2.5 × 4 cm^2) redox electrodes that had been activated beforehand as described above. The primary Ni electrodes (anode and cathode) were dipped in two glass bottles filled with alkaline aqueous solution (1 M NaOH in deionized water) and connected to a potentiostat/galvanostat. Two-electrode experiments were performed by attaching the counter and reference electrodes together, thereby giving a floating reference configuration. The redox electrodes were placed in the respective bottles in proximity to the primary electrodes (1.5 cm). The CuO-$Cu(OH)_2$ electrode was placed close to the Ni anode in the oxygen cell. And finally, the Cu_2O electrode was placed close to the Ni cathode in the hydrogen cell. The duration time of electrolysis cycles was 1 h with an applied constant voltage of 2–3 V. The threshold limit was set at 3 V to avoid gas generation at the redox mediator electrodes.

Performance of the Two-Cell Water Electrolysis System and Photoenhanced Pure Gas Production. To measure the gas volume and Faradaic efficiency of the total water electrolysis process at a constant applied voltage of 2 V in the two-electrode system, the volume of H_2 and O_2 production was measured using a custom-built device (shown in Supplementary Figure S8b). The mixing of gases during water electrolysis was monitored by an in situ gas chromatography technique. Before all gas analyses, the electrolyte and seal cells were purged with pure Ar (99%) or N_2 (99%) and pumped down to vacuum in several pump–purge cycles.

For the photoenhanced gas production measurement, the redox mediator electrode was exposed to simulate sunlight from the solar simulator. The light was reflected from a mirror and projected onto the sample (illumination area 10 cm^2) with

an intensity of 80 mW/cm^2. The photoresponse of mediator electrodes during water electrolysis was performed under on–off light irradiation.

In Situ X-ray Absorption Spectroscopy (XAS). The Cu K-edge X-ray absorption experiments were conducted in fluorescent mode at BL5.2 of the Synchrotron Light Research Institute (SLRI), Thailand. The electron energy was 1.2 GeV, the beam current was 80–150 mA, and the maximum photon flux was about 1.1–1.7 × 10^{11} photons s^{-1}. The X-ray beam size was 25 mm (width) × 1 mm (height). To record XANES and EXAFS spectra in fluorescence mode, a four-channel Si detector after calibration with a Cu foil was used. The measurement parameters were adjusted to achieve a reliable dead time below 10% (1 s). The normalized XAS spectra were processed and analyzed by using the Athena and Artemis software. For in situ XANES and EXAFS measurements, all spectra were collected during water electrolysis in the two-cell setup. The electrolysis cell was made of acrylic material with dimensions of 5 × 5 × 7 cm^3 and a square hole (3 × 3 cm^2) with Kapton tape as the entrance of the X-ray beam. The measurement was operated at a constant voltage of 3 V in both the presence and absence of laser light irradiation (450 nm, 80 mW/cm^2) on mediator electrodes.

Photoemission Spectroscopy (PES). To understand the influence of light during electrolysis, the electronic structures of the mediator electrodes under laser light irradiation (450 nm, 80 mW/cm^2) were investigated by using ultraviolet photoemission spectroscopy (UPS) at room temperature with a photon energy of 90 eV (electron mean free path ≈ 5.5 Å) and a pass energy of 5 eV. The base pressure was better than 1 × 10^{-8} mbar. The valence band spectra were collected on a Scienta R4000 analyzer with an energy resolution of 30 meV at BL3.2a of the Synchrotron Light Research Institute (SLRI), Thailand. In addition, the elemental compositions of the electrodes in all conditions were analyzed by X-ray photoelectron spectroscopy (XPS) using an PHI5000 Versa Probe II (Ulvac-PHI, Japan) with Al Kα radiation (photon energy 1486.6 eV) at BL5.3 of SLRI.

ASSOCIATED CONTENT

Ⓢ Supporting Information

The Supporting Information is available free of charge at https://pubs.acs.org/doi/10.1021/acsomega.1c02305.

> The surface morphologies of the CuO-Cu(OH)$_2$ electrode, EDS and XRD analysis, electrochemical impedance spectroscopy study, the operation of the two-cell water electrolysis system, electrochemical properties, gas measurement and Faradaic efficiency, in situ gas chromatography, gas production of the two-cell water electrolysis under dark and light illumination, photoemission spectroscopy analysis, and proposed mechanism of charge transfer (PDF)

AUTHOR INFORMATION

Corresponding Author

Worawat Meevasana − *Research Network NANOTEC-SUT on Advanced Nanomaterials and Characterization and School of Physics, Suranaree University of Technology, Nakhon Ratchasima 30000, Thailand; Thailand Center of Excellence in Physics, Ministry of Higher Education, Science, Research and Innovation, Bangkok 10400, Thailand;*

 orcid.org/0000-0003-2994-6249; Email: worawat@ g.sut.ac.th

Authors

Supansa Musikajaroen − *Research Network NANOTEC-SUT on Advanced Nanomaterials and Characterization and School of Physics, Suranaree University of Technology, Nakhon Ratchasima 30000, Thailand; Thailand Center of Excellence in Physics, Ministry of Higher Education, Science, Research and Innovation, Bangkok 10400, Thailand*

Siwat Polin − *Research Network NANOTEC-SUT on Advanced Nanomaterials and Characterization and School of Physics, Suranaree University of Technology, Nakhon Ratchasima 30000, Thailand*

Suchinda Sattayaporn − *Synchrotron Light Research Institute, Nakhon Ratchasima 30000, Thailand*

Warakorn Jindata − *Research Network NANOTEC-SUT on Advanced Nanomaterials and Characterization and School of Physics, Suranaree University of Technology, Nakhon Ratchasima 30000, Thailand*

Wittawat Saenrang − *Research Network NANOTEC-SUT on Advanced Nanomaterials and Characterization and School of Physics, Suranaree University of Technology, Nakhon Ratchasima 30000, Thailand; Thailand Center of Excellence in Physics, Ministry of Higher Education, Science, Research and Innovation, Bangkok 10400, Thailand*

Pinit Kidkhunthod − *Synchrotron Light Research Institute, Nakhon Ratchasima 30000, Thailand*

Hideki Nakajima − *Synchrotron Light Research Institute, Nakhon Ratchasima 30000, Thailand*

Teera Butburee − *National Nanotechnology Center, National Science and Technology Development Agency, Pathum Thani 12120, Thailand*

Narong Chanlek − *Synchrotron Light Research Institute, Nakhon Ratchasima 30000, Thailand*

Complete contact information is available at:
https://pubs.acs.org/10.1021/acsomega.1c02305

Author Contributions

W.M. conceived and guided the entire project. S.M. and S.P. designed and set up the experiment. S.M. performed the experiment and analyzed the data. H.N. and N.C. took the XPS/UPS measurement. S.S. and P.K. took and analyzed the XAS data. W.M. and S.M. wrote the manuscript. All authors participated in discussion of the results, commented on the manuscript, and have given approval to the final version of the manuscript. W.M. directed the research.

Notes

The authors declare no competing financial interest.

ACKNOWLEDGMENTS

■ REFERENCES

(1) Holladay, J. D.; Hu, J.; King, D. L.; Wang, Y. An overview of hydrogen production technologies. *Catal. Today* **2009**, *139*, 244−260.

(2) Shiva Kumar, S.; Himabindu, V. Hydrogen production by PEM water electrolysis − A review. *Mater. Sci. Energy Technol.* **2019**, *2*, 442−454.

(3) Wang, S.; Lu, A.; Zhong, C.-J. Hydrogen production from water electrolysis: role of catalysts. *Nano Converg.* **2021**, *8*, 4.

(4) Landman, A.; Dotan, H.; Shter, G. E.; Wullenkord, M.; Houaijia, A.; Maljusch, A.; Grader, G. S.; Rothschild, A. Photoelectrochemical water splitting in separate oxygen and hydrogen cells. *Nat. Mater.* **2017**, *16*, 646.

(5) Landman, A.; Halabi, R.; Dias, P.; Dotan, H.; Mehlmann, A.; Shter, G. E.; Halabi, M.; Naseraldeen, O.; Mendes, A.; Grader, G. S.; Rothschild, A. Decoupled Photoelectrochemical Water Splitting System for Centralized Hydrogen Production. *Joule* **2020**, *4*, 448−471.

(6) Goodwin, S.; Walsh, D. A. Closed Bipolar Electrodes for Spatial Separation of H_2 and O_2 Evolution during Water Electrolysis and the Development of High-Voltage Fuel Cells. *ACS Appl. Mater. Interfaces* **2017**, *9*, 23654−23661.

(7) Scheepers, F.; Stähler, M.; Stähler, A.; Rauls, E.; Müller, M.; Carmo, M.; Lehnert, W. Improving the Efficiency of PEM Electrolyzers through Membrane-Specific Pressure Optimization. *Energies* **2020**, *13*, 612.

(8) Chen, L.; Dong, X.; Wang, Y.; Xia, Y. Separating hydrogen and oxygen evolution in alkaline water electrolysis using nickel hydroxide. *Nat. Commun.* **2016**, *7*, 11741.

(9) Rausch, B.; Symes, M. D.; Chisholm, G.; Cronin, L. Decoupled catalytic hydrogen evolution from a molecular metal oxide redox mediator in water splitting. *Science* **2014**, *345*, 1326.

(10) Symes, M. D.; Cronin, L. Decoupling hydrogen and oxygen evolution during electrolytic water splitting using an electron-coupled-proton buffer. *Nat. Chem.* **2013**, *5*, 403.

(11) You, B.; Sun, Y. Innovative Strategies for Electrocatalytic Water Splitting. *Acc. Chem. Res.* **2018**, *51*, 1571−1580.

(12) Hou, M.; Chen, L.; Guo, Z.; Dong, X.; Wang, Y.; Xia, Y. A clean and membrane-free chlor-alkali process with decoupled Cl_2 and H_2/NaOH production. *Nat. Commun.* **2018**, *9*, 438.

(13) Dotan, H.; Landman, A.; Sheehan, S. W.; Malviya, K. D.; Shter, G. E.; Grave, D. A.; Arzi, Z.; Yehudai, N.; Halabi, M.; Gal, N.; Hadari, N.; Cohen, C.; Rothschild, A.; Grader, G. S. Decoupled hydrogen and oxygen evolution by a two-step electrochemical−chemical cycle for efficient overall water splitting. *Nat. Energy* **2019**, *4*, 786−795.

(14) Ahmad Kamaroddin, M. F.; Sabli, N.; Tuan Abdullah, T. A. *Hydrogen Production by Membrane Water Splitting Technologies*; IntechOpen: 2018, 19.

(15) Lamy, C. From hydrogen production by water electrolysis to its utilization in a PEM fuel cell or in a SO fuel cell: Some considerations on the energy efficiencies. *Int. J. Hydrogen Energy* **2016**, *41*, 15415−15425.

(16) Senthilkumar, V.; Kim, Y. S.; Chandrasekaran, S.; Rajagopalan, B.; Kim, E. J.; Chung, J. S. Comparative supercapacitance performance of CuO nanostructures for energy storage device applications. *RSC Adv.* **2015**, *5*, 20545−20553.

(17) Xu, L.; Li, J.; Sun, H.; Guo, X.; Xu, J.; Zhang, H.; Zhang, X. In situ Growth of Cu_2O/CuO Nanosheets on Cu Coating Carbon Cloths as a Binder-Free Electrode for Asymmetric Supercapacitors. *Front. Chem.* **2019**, *7*, 420.

(18) Xu, P.; Liu, J.; Liu, T.; Ye, K.; Cheng, K.; Yin, J.; Cao, D.; Wang, G.; Li, Q. Preparation of binder-free CuO/Cu_2O/Cu composites: a novel electrode material for supercapacitor applications. *RSC Adv.* **2016**, *6*, 28270−28278.

(19) Xu, P.; Ye, K.; Du, M.; Liu, J.; Cheng, K.; Yin, J.; Wang, G.; Cao, D. One-step synthesis of copper compounds on copper foil and their supercapacitive performance. *RSC Adv.* **2015**, *5*, 36656−36664.

(20) An, C.; Wang, Z.; Xi, W.; Wang, K.; Liu, X.; Ding, Y. Nanoporous $Cu@Cu_2O$ hybrid arrays enable photo-assisted supercapacitor with enhanced capacities. *J. Mater. Chem. A* **2019**, *7*, 15691−15697.

(21) Kalasina, S.; Pattanasattayavong, P.; Suksomboon, M.; Phattharasupakun, N.; Wutthiprom, J.; Sawangphruk, M. A new concept of charging supercapacitors based on the photovoltaic effect. *Chem. Commun.* **2017**, *53*, 709−712.

(22) Kalasina, S.; Phattharasupakun, N.; Maihom, T.; Promarak, V.; Sudyoadsuk, T.; Limtrakul, J.; Sawangphruk, M. Novel Hybrid Energy Conversion and Storage Cell with Photovoltaic and Supercapacitor Effects in Ionic Liquid Electrolyte. *Sci. Rep.* **2018**, *8*, 12192.

(23) Safshekan, S.; Herraiz-Cardona, I.; Cardenas-Morcoso, D.; Ojani, R.; Haro, M.; Gimenez, S. Solar Energy Storage by a Heterostructured $BiVO_4$−PbO_x Photocapacitive Device. *ACS Energy Lett.* **2017**, *2*, 469−475.

(24) Xia, X.; Luo, J.; Zeng, Z.; Guan, C.; Zhang, Y.; Tu, J.; Zhang, H.; Fan, H. J. Integrated photoelectrochemical energy storage: solar hydrogen generation and supercapacitor. *Sci. Rep.* **2012**, *2*, 981.

(25) Dias, P.; Schreier, M.; Tilley, S. D.; Luo, J.; Azevedo, J.; Andrade, L.; Bi, D.; Hagfeldt, A.; Mendes, A.; Grätzel, M.; Mayer, M. T. Transparent Cuprous Oxide Photocathode Enabling a Stacked Tandem Cell for Unbiased Water Splitting. *Adv. Energy Mater.* **2015**, *5*, 1501537.

(26) Luo, J.; Steier, L.; Son, M.-K.; Schreier, M.; Mayer, M. T.; Grätzel, M. Cu_2O Nanowire Photocathodes for Efficient and Durable Solar Water Splitting. *Nano Lett.* **2016**, *16*, 1848−1857.

(27) Shu, X.; Zheng, H.; Xu, G.; Zhao, J.; Cui, L.; Cui, J.; Qin, Y.; Wang, Y.; Zhang, Y.; Wu, Y. The anodization synthesis of copper oxide nanosheet arrays and their photoelectrochemical properties. *Appl. Surf. Sci.* **2017**, *412*, 505−516.

(28) Zhang, Z.; Wang, P. Highly stable copper oxide composite as an effective photocathode for water splitting via a facile electrochemical synthesis strategy. *J. Mater. Chem.* **2012**, *22*, 2456−2464.

(29) Guan, B.-J.; van Hoef, V.; Jobava, R.; Elroy-Stein, O.; Valasek, L. S.; Cargnello, M.; Gao, X.-H.; Krokowski, D.; Merrick, W. C.; Kimball, S. R.; Komar, A. A.; Koromilas, A. E.; Wynshaw-Boris, A.; Topisirovic, I.; Larsson, O.; Hatzoglou, M. A Unique ISR Program Determines Cellular Responses to Chronic Stress. *Mol. Cell* **2017**, *68*, 885−900.e6.

(30) Zaafarany, I.; Boller, H. Electrochemical behavior of copper electrode in sodium hydroxide solutions. *Curr. World Environ.* **2009**, *4*, 277−284.

(31) Wang, Y.-H.; He, J.-B. Corrosion inhibition of copper by sodium phytate in NaOH solution: Cyclic voltabsorptometry for in situ monitoring of soluble corrosion products. *Electrochim. Acta* **2012**, *66*, 45−51.

(32) Pongha, S.; Seekoaon, B.; Limphirat, W.; Kidkhunthod, P.; Srilomsak, S.; Chiang, Y.-M.; Meethong, N. XANES Investigation of Dynamic Phase Transition in Olivine Cathode for Li-Ion Batteries. *Adv. Energy Mater.* **2015**, *5*, 1500663.

(33) Xuning, L.; Wang, H.-Y.; Yang, H.; Cai, W.; Liu, S.; Liu, B. In Situ/Operando Characterization Techniques to Probe the Electrochemical Reactions for Energy Conversion. *Small Methods* **2018**, 1700395.

(34) Aregahegn, A.; Gedamu, A.; Chen, H.-M.; Berhe, T.; Su, W.-N.; Hwang, B. J. Highly stable CuS and CuS-Pt catalyzed Cu_2O/CuO heterostructure as efficient photocathode for hydrogen evolution reaction. *J. Mater. Chem. A* **2015**, *4*, 2205.

(35) Dubale, A. A.; Pan, C.-J.; Tamirat, A. G.; Chen, H.-M.; Su, W.-N.; Chen, C.-H.; Rick, J.; Ayele, D. W.; Aragaw, B. A.; Lee, J.-F.; Yang, Y.-W.; Hwang, B.-J. Heterostructured Cu_2O/CuO decorated with nickel as a highly efficient photocathode for photoelectrochemical water reduction. *J. Mater. Chem. A* **2015**, *3*, 12482−12499.

(36) Wang, Y.; Lany, S.; Ghanbaja, J.; Fagot-Revurat, Y.; Chen, Y. P.; Soldera, F.; Horwat, D.; Mücklich, F.; Pierson, J. F. Electronic structures of Cu_2O, Cu_3O_4 and CuO: A joint experimental and theoretical study. *Phys. Rev. B* **2016**, *94*, 245418.

(37) Yang, Y.; Xu, D.; Wu, Q.; Diao, P. Cu_2O/CuO Bilayered Composite as a High-Efficiency Photocathode for Photoelectrochemical Hydrogen Evolution Reaction. *Sci. Rep.* **2016**, *6*, 35158.

(38) Aguirre, M. E.; Zhou, R.; Eugene, A. J.; Guzman, M. I.; Grela, M. A. Cu_2O/TiO_2 heterostructures for CO_2 reduction through a direct Z-scheme: Protecting Cu_2O from photocorrosion. *Appl. Catal., B* **2017**, *217*, 485−493.

(39) Huang, L.; Peng, F.; Yu, H.; Wang, H. Preparation of cuprous oxides with different sizes and their behaviors of adsorption, visible-light driven photocatalysis and photocorrosion. *Solid State Sci.* **2009**, *11*, 129−138.

(40) Kakuta, S.; Abe, T. Structural characterization of Cu_2O after the evolution of H_2 under visible light irradiation. *Electrochem. Solid-State Lett.* **2009**, *12*, P1−P3.

(41) Saratale, R. G.; Ghodake, G. S.; Shinde, S. K.; Cho, S.-K.; Saratale, G. D.; Pugazhendhi, A.; Bharagava, R. N. Photocatalytic activity of $CuO/Cu(OH)_2$ nanostructures in the degradation of Reactive Green 19A and textile effluent, phytotoxicity studies and their biogenic properties (antibacterial and anticancer). *J. Environ. Manage.* **2018**, *223*, 1086−1097.

(42) Toe, C. Y.; Scott, J.; Amal, R.; Ng, Y. H. Recent advances in suppressing the photocorrosion of cuprous oxide for photocatalytic and photoelectrochemical energy conversion. *J. Photochem. Photobiol., C* **2018**, 191.

(43) Zheng, Z.; Huang, B.; Wang, Z.; Guo, M.; Qin, X.; Zhang, X.; Wang, P.; Dai, Y. Crystal Faces of Cu_2O and Their Stabilities in Photocatalytic Reactions. *J. Phys. Chem. C* **2009**, *113*, 14448−14453.

(44) Yoshida, M.; Yomogida, T.; Mineo, T.; Nitta, K.; Kato, K.; Masuda, T.; Nitani, H.; Abe, H.; Takakusagi, S.; Uruga, T.; Asakura, K.; Uosaki, K.; Kondoh, H. Photoexcited Hole Transfer to a MnO_x Cocatalyst on a $SrTiO_3$ Photoelectrode during Oxygen Evolution Studied by In Situ X-ray Absorption Spectroscopy. *J. Phys. Chem. C* **2014**, *118*, 24302−24309.

(45) van Oversteeg, C. H. M.; Doan, H. Q.; de Groot, F. M. F.; Cuk, T. In situ X-ray absorption spectroscopy of transition metal based water oxidation catalysts. *Chem. Soc. Rev.* **2017**, *46*, 102−125.

(46) Xiao, Z.; Wang, Y.; Huang, Y.-C.; Wei, Z.; Dong, C.-L.; Ma, J.; Shen, S.; Li, Y.; Wang, S. Filling the oxygen vacancies in Co_3O_4 with phosphorus: an ultra-efficient electrocatalyst for overall water splitting. *Energy Environ. Sci.* **2017**, *10*, 2563−2569.

(47) Zhang, Y.-C.; Afzal, N.; Pan, L.; Zhang, X.; Zou, J.-J. Structure-Activity Relationship of Defective Metal-Based Photocatalysts for Water Splitting: Experimental and Theoretical Perspectives. *Adv. Sci.* **2019**, *6*, 1900053.

(48) Masingboon, C.; Eknapakul, T.; Suwanwong, S.; Buaphet, P.; Nakajima, H.; Mo, S.-K.; Thongbai, P.; King, P. D. C.; Maensiri, S.; Meevasana, W. Anomalous change in dielectric constant of $CaCu_3Ti_4O_{12}$ under violet-to-ultraviolet irradiation. *Appl. Phys. Lett.* **2013**, *102*, 202903.

(49) Meevasana, W.; King, P. D. C.; He, R. H.; Mo, S. K.; Hashimoto, M.; Tamai, A.; Songsiriritthigul, P.; Baumberger, F.; Shen, Z. X. Creation and control of a two-dimensional electron liquid at the bare $SrTiO_3$ surface. *Nat. Mater.* **2011**, *10*, 114.

(50) Suwanwong, S.; Eknapakul, T.; Rattanachai, Y.; Masingboon, C.; Rattanasuporn, S.; Phatthanakun, R.; Nakajima, H.; King, P. D. C.; Hodak, S. K.; Meevasana, W. The dynamics of ultraviolet-induced oxygen vacancy at the surface of insulating $SrTiO_3(001)$. *Appl. Surf. Sci.* **2015**, *355*, 210−212.

(51) Singh, M.; Jampaiah, D.; Kandjani, A. E.; Sabri, Y. M.; Della Gaspera, E.; Reineck, P.; Judd, M.; Langley, J.; Cox, N.; van Embden, J.; Mayes, E. L. H.; Gibson, B. C.; Bhargava, S. K.; Ramanathan, R.; Bansal, V. Oxygen-deficient photostable Cu_2O for enhanced visible light photocatalytic activity. *Nanoscale* **2018**, *10*, 6039−6050.

(52) Nathabumroong, S.; Eknapakul, T.; Jaiban, P.; Yotburut, B.; Siriroj, S.; Saisopa, T.; Mo, S. K.; Supruangnet, R.; Nakajima, H.; Yimnirun, R.; Maensiri, S.; Meevasana, W. Interplay of negative electronic compressibility and capacitance enhancement in lightly-doped metal oxide $Bi_{0.95}La_{0.05}FeO_3$ by quantum capacitance model. *Sci. Rep.* **2020**, *10*, 5153.

(53) Liu, J.; Ke, J.; Li, D.; Sun, H.; Liang, P.; Duan, X.; Tian, W.; Tadé, M. O.; Liu, S.; Wang, S. Oxygen Vacancies in Shape Controlled $Cu_2O/Reduced$ Graphene Oxide/In_2O_3 Hybrid for Promoted Photocatalytic Water Oxidation and Degradation of Environmental Pollutants. *ACS Appl. Mater. Interfaces* **2017**, *9*, 11678−11688.

(54) Khan, M. E.; Khan, M. M.; Cho, M. H. Ce^{3+}-ion, Surface oxygen vacancy, and visible light-induced photocatalytic dye degradation and photocapacitive performance of CeO_2-graphene nanostructures. *Sci. Rep.* **2017**, *7*, 5928.

(55) Liu, Q.; Wang, F.; Lin, H.; Xie, Y.; Tong, N.; Lin, J.; Zhang, X.; Zhang, Z.; Wang, X. Surface oxygen vacancy and defect engineering of WO_3 for improved visible light photocatalytic performance. *Catal. Sci. Technol.* **2018**, *8*, 4399−4406.

(56) Lv, Y.; Yao, W.; Zong, R.; Zhu, Y. Fabrication of Wide−Range−Visible Photocatalyst $Bi_2WO_{6−x}$ nanoplates via Surface Oxygen Vacancies. *Sci. Rep.* **2016**, *6*, 19347.

(57) Zhao, J.; Li, Z.; Shen, T.; Yuan, X.; Qiu, G.; Jiang, Q.; Lin, Y.; Song, G.; Meng, A.; Li, Q. Oxygen-vacancy Bi_2O_3 nanosheet arrays with excellent rate capability and $CoNi_2S_4$ nanoparticles immobilized on N-doped graphene nanotubes as robust electrode materials for high-energy asymmetric supercapacitors. *J. Mater. Chem. A* **2019**, *7*, 7918−7931.

(58) Lu, L.; Xu, X.; Yan, J.; Shi, F.-N.; Huo, Y. Oxygen vacancy rich Cu_2O based composite material with nitrogen doped carbon as matrix for photocatalytic H_2 production and organic pollutant removal. *Dalton Trans.* **2018**, *47*, 2031−2038.

(59) Yan, Y.; Shi, W.; Peng, W.; Lin, Y.; Zhang, C.; Li, L.; Sun, Y.; Ju, H.; Zhu, J.; Ma, W.; Zhao, J. Proton-free electron-trapping feature of titanium dioxide nanoparticles without the characteristic blue color. *Commun. Chem.* **2019**, *2*, 88.

(60) Cheng, Y.; Lin, Y.; Xu, J.; He, J.; Wang, T.; Yu, G.; Shao, D.; Wang, W.-H.; Lu, F.; Li, L.; Du, X.; Wang, W.; Liu, H.; Zheng, R. Surface plasmon resonance enhanced visible-light-driven photocatalytic activity in Cu nanoparticles covered Cu_2O microspheres for degrading organic pollutants. *Appl. Surf. Sci.* **2016**, *366*, 120−128.